Boost the immune response with
**High-quality PRR ligands**

InvivoGen

# The Journal of Immunology

This information is current as of October 13, 2016.

## Accelerated Turnover of MHC Class II Molecules in Nonobese Diabetic Mice Is Developmentally and Environmentally Regulated In Vivo and Dispensable for Autoimmunity

Alessandra De Riva, Mark C. Varley, Leslie J. Bluck, Anne Cooke, Michael J. Deery and Robert Busch

| | |
|---|---|
| **Supplementary Material** | http://www.jimmunol.org/content/suppl/2013/05/17/jimmunol.1300551.DC1.html |
| **References** | This article **cites 49 articles**, 21 of which you can access for free at: http://www.jimmunol.org/content/190/12/5961.full#ref-list-1 |
| **Subscriptions** | Information about subscribing to *The Journal of Immunology* is online at: http://jimmunol.org/subscriptions |
| **Permissions** | Submit copyright permission requests at: http://www.aai.org/ji/copyright.html |
| **Email Alerts** | Receive free email-alerts when new articles cite this article. Sign up at: http://jimmunol.org/cgi/alerts/etoc |

# Accelerated Turnover of MHC Class II Molecules in Nonobese Diabetic Mice Is Developmentally and Environmentally Regulated In Vivo and Dispensable for Autoimmunity

Alessandra De Riva,* Mark C. Varley,*,† Leslie J. Bluck,‡ Anne Cooke,§ Michael J. Deery,¶ and Robert Busch*

The H2-A$^{g7}$ (A$^{g7}$) MHC class II (MHCII) allele is required for type 1 diabetes (T1D) in NOD mice. A$^{g7}$ not only has a unique peptide-binding profile, it was reported to exhibit biochemical defects, including accelerated protein turnover. Such defects were proposed to impair Ag presentation and, thus, self-tolerance. Here, we report measurements of MHCII protein synthesis and turnover in vivo. NOD mice and BALB/c controls were labeled continuously with heavy water, and splenic B cells and dendritic cells were isolated. MHCII molecules were immunoprecipitated and digested with trypsin. Digests were analyzed by liquid chromatography/mass spectrometry to quantify the fraction of newly synthesized MHCII molecules and, thus, turnover. MHCII turnover was faster in dendritic cells than in B cells, varying slightly between mouse strains. Some A$^{g7}$ molecules exhibited accelerated turnover in B cells from young, but not older, prediabetic female NOD mice. This acceleration was not detected in a second NOD colony with a high incidence of T1D. Turnover rates of A$^{g7}$ and H2-A$^{d}$ were indistinguishable in (NOD × BALB/c) F1 mice. In conclusion, accelerated MHCII turnover may occur in NOD mice, but it reflects environmental and developmental regulation, rather than a structural deficit of the A$^{g7}$ allele. Moreover, this phenotype wanes before the onset of overt T1D and is dispensable for the development of autoimmune diabetes. Our observations highlight the importance of in vivo studies in understanding the role of protein turnover in genotype/phenotype relationships and offer a novel approach for addressing this fundamental research challenge. *The Journal of Immunology*, 2013, 190: 5961–5971.

N onobese diabetic mice have been studied extensively as a paradigm of complex autoimmune disease, which develops under the control of genetic, hormonal, and environmental influences. Lymphocyte infiltration of pancreatic islets develops at a young age, leading to progressive β cell destruction and, starting around 12 wk of age, to overt type 1 diabetes (T1D), with a female sex bias (1). Genetic control of T1D in NOD mice includes critical contributions from both H2-A and H2-E MHC class II (MHCII) loci, alongside multiple non-MHCII genes, most of which affect T cell function (2, 3). NOD mice lack Eα transcription; in addition, the unique H2-A$^{g7}$ (A$^{g7}$) β-chain differs by 17 aa from the protective Aβ$^{d}$ allele (4). T1D development is reduced or abrogated in NOD mice transgenic for Eα or other H2-A alleles (3). MHCII glyco-proteins normally present peptides to CD4$^+$ T lymphocytes, and NOD mice harbor pathogenic CD4$^+$ effector T cells that recognize islet autoantigens presented by A$^{g7}$ (reviewed in Ref. 5). Aβ$^{g7}$ shares key polymorphisms, in particular a non-Asp residue at position 57, and peptide-binding preferences with human HLA-DQB1 alleles that confer risk for T1D (6–8). Nonetheless, no unifying explanation for the link between these alleles and islet autoimmunity has emerged from considerations of peptide-binding specificity (5). Moreover, the potential for A$^{g7}$-restricted T cell autoreactivity extends to self-Ags that are systemically expressed, both in the "autoproliferation" phenotype of NOD mice (9, 10) and in the K/ B×N model of autoimmune arthritis (11, 12). These considerations prompted suggestions that A$^{g7}$ confers a broader tendency toward autoreactivity, perhaps mediated by unique biochemical properties other than their peptide-binding specificity.

Indeed, A$^{g7}$ exhibits several unusual biochemical properties compared with other MHCII alleles (5). Many MHCII alleles re-main stable as αβ heterodimers in SDS at room temperature when loaded stably with peptides, but A$^{g7}$ dimers readily dissociate under these conditions (13). Genetic studies indicate that this relative instability represents an intrinsic structural property of the A$^{g7}$ heterodimer. SDS instability also correlates with the T1D risk or protection associated with human DQ alleles (14). In [$^{35}$S]-pulse/chase experiments performed in vitro, A$^{g7}$ exhibited faster turnover in cultured NOD splenocytes than did other H2-A alleles in splenocytes from other mouse strains (13). Based on these observations, it was proposed that a biochemical stability defect of

*Department of Medicine, University of Cambridge, Addenbrooke's Hospital, Cambridge CB2 0QQ, United Kingdom; †Department of Engineering, University of Cambridge, Cambridge CB2 1PZ, United Kingdom; ‡Elsie Widdowson Laboratories, Medical Research Council Human Nutrition Research, Fulbourn, Cambridge CB1 9NL, United Kingdom; §Department of Pathology, University of Cambridge, Cambridge CB2 1QP, United Kingdom; and ¶Cambridge Centre for Proteomics, University of Cambridge, Cambridge CB2 1QR, United Kingdom

$A^{g7}$, leading to accelerated turnover, might impair T cell tolerance (9, 10).

This view has been controversial, however. SDS instability is shared by other H2-A alleles, which are not associated with spontaneous autoimmunity; $A^{g7}$ may be at the lower end of normal allelic variation in this regard (5, 15). Initial evidence that SDS instability was attributable to poor peptide binding by $A^{g7}$ (13) was not borne out by subsequent peptide-binding and extraction studies (5). Moreover, several HLA-DQ alleles that confer risk for T1D in humans retain peptides well, despite interacting poorly with HLA-DM during endosomal peptide loading (5). Structural studies in which $A^{g7}$ was expressed and crystallized did not indicate any marked defects in stability or folding (16).

More recent studies showed that MHCII protein life span is affected by extrinsic variables. Wild-type APCs of different lineages vary in their MHCII-internalization rates, correlating with the length of ubiquitin chains attached to MHCII β-chains (17). Ubiquitination is modulated during activation of dendritic cells (DCs) by proinflammatory stimuli in vitro (18), correlating with large differences in MHCII protein life span (19). Genetic deficiency in the peptide-exchange cofactor, DM, reduces the surface expression of $A^{g7}$ and other MHCII alleles with low affinity for invariant chain peptides and increases their turnover (20, 21). Similar effects on MHCII life span could result from negative regulation of DM activity by HLA-DO/H2-DO (22), which is differentially expressed during APC development (23–25). In NOD mice, MHCII associations with invariant chain may be abnormal, and the development and frequencies of B cells and DCs were reported to be altered, with unknown consequences for the regulation of MHCII protein life span (5).

Moreover, T1D development is subject to environmental control. In NOD colonies worldwide, T1D incidence varies between from ~20 to ≥80% in females at 30 wk of age (26), suggesting that diabetes development is influenced by environmental and epigenetic factors. Environmental factors that contribute to this variation include multiple viral, bacterial, and eukaryotic pathogens; the resident intestinal microflora; as well as experimentally administered proinflammatory stimuli, all of which modify host immune responsiveness (27). In addition, hormonal regulation is suggested by the much lower disease incidence in males; this, too, is influenced by the microbiome (28). Whether disease-relevant environmental factors affect MHCII protein life span in vivo remains unclear.

A definitive assessment of the determinants of MHCII protein instability and its role in autoimmune pathogenesis requires quantification of turnover rates in vivo in APCs of living animals. Methodologies for addressing this problem have been lacking until recently. Radiolabeling, a standard approach for measuring protein life span in vitro (29), is difficult to use in vivo. Stable isotope labeling of amino acids in cell culture (SILAC) has been applied in vivo, but complete labeling of proteins with essential amino acids takes several generations in mice (30), and the precursor/product relationships are not well understood in vivo. Stable isotope approaches have been used for proteome-wide surveys of steady-state protein expression levels and for kinetic proteomics; in contrast, little work has focused on assessing the effects of structural polymorphism on the turnover rates of specific proteins of interest.

We (31, 32) and, independently, other investigators (33, 34) developed an alternative approach to address this problem: stable isotope labeling of nonessential amino acids with heavy water (SINEW). We showed that this approach can be used to quantify the biosynthetic dynamics of different MHC allotypes (31). Deuterated water (heavy water, $^2H_2O$) is used as a nonradioactive metabolic tracer, which does not interfere detectably with normal physiology at the concentrations used for labeling (35). Following $^2H_2O$ administration, $^2H$ equilibrates rapidly across body water pools and is incorporated biosynthetically into nonessential amino acids and, hence, into proteins of interest (31, 32), with minimal and transient interference from dietary amino acids (32, 36). The approach is now well-validated for quantification of protein synthesis on time scales of a few hours or longer. In this study, we applied SINEW to characterize MHCII turnover in vivo. Surprisingly, our findings indicate that environmental and developmental variables, rather than structural polymorphism, are key determinants of accelerated turnover of $A^{g7}$ in NOD APCs and that this phenotype is dispensable for development of T1D.

## Materials and Methods

### Mice and cell lines

Animal studies were performed according to institutional and national guidelines under UK Home Office Project Licenses 80/2156 and 80/2440. For most studies, NOD mice (named "$NOD^{low}$" where necessary to avoid ambiguity) were bred under specific pathogen–free conditions at the Centre for Biomedical Services, University of Cambridge, from founder stock kindly provided by Prof. Linda Wicker. NOD genotype (100%) was authenticated in a breeding trio using an array of 384 single nucleotide polymorphisms (Charles River Laboratories), spaced ~7 MB apart across the entire genome, which distinguish common inbred mouse strains. BALB/c mice were purchased from Charles River Laboratories and used after 10 d of acclimatization in the same facility. Female BALB/c mice were bred with NOD males to generate F1 mice. Animals were maintained in individually ventilated cages and received standard rodent chow and water ad libitum.

A second colony of NOD mice (named "$NOD^{high}$") was bred in the animal facility of the Department of Pathology, University of Cambridge, and maintained under barrier conditions. These NOD mice were also derived from founder stock kindly provided by Prof. Linda Wicker in 2002. T1D incidence increased over time in the facility in the Department of Pathology and subsequently remained high (≥80% by 30 wk of age in females).

Both colonies were maintained by breeding the first litter in each generation and were kept on the same diet. For incidence studies, animals were aged to 30 wk and observed regularly for signs of diabetes; incidence was confirmed by measurement of glucosuria, using Diastix (Bayer Diagnostics). Routine veterinary microbiological screening of sentinel mice in both colonies was carried out to a standard exceeding current recommendations of the Federation of European Laboratory Animal Sciences Associations (B&K Diagnostics).

M12.NOD is a derivative of the M12 murine B lymphoma cell line transfected with $A^{g7}$ genes. These cells, as well as murine A20 B lymphoma cells and the EBV-transformed B cell line, Priess, were cultured as previously described (31).

### Labeling experiments

Mice were labeled to 4–5 atom percent enrichment (a.p.e.) of $^2H_2O$ in body water by initial i.p. bolus injection of 35 ml/kg 99% a.p.e. $^2H_2O$ (CK Gas) containing 0.9% w/v NaCl. This material was depleted of LPS using Detoxi-Gel Columns (Thermo Scientific) and sterile filtered. The initial body water enrichment was maintained by continuous administration of 8% a.p.e. $^2H_2O$ in drinking water ad libitum. Control animals received injections of LPS-depleted 0.9% (w/v) NaCl in natural-abundance water and were maintained concurrently. At various time points following i.p. bolus, animals were exsanguinated under terminal general anesthesia, and spleens and femurs were removed following cervical dislocation.

### Abs

MK-D6 (IgG2a anti–H2-A$^d$) (37) and 14.4.4S (IgG2a anti–H2-E) (38) hybridomas were kind gifts from Dr. B. Stockinger. ME-1 (IgG1 anti–HLA-B27) (39) and W6/32 (IgG2a anti–HLA-A/-B/-C) (40) were kindly provided by Prof. J.S.H. Gaston and used as isotype controls. The mAbs were used as culture supernatants or purified over protein A or protein G affinity columns (GE Biosciences). For flow cytometry, MK-D6 was FITC labeled using Lightning-Link Fluorescein (Innova Biosciences). Other Abs (developed in mice, unless mentioned otherwise) were obtained commercially: IgG1-FITC isotype control, clone MOPC21, from BD Biosciences; IgG2a-FITC isotype control, cat no. MG2A01, from Invitrogen; and CD19-PE/Cy5, clone eBio1D3, and rat anti-mouse CD86-PE, clone PO3.1,

from eBioscience. The following Abs were from BioLegend: CD11c–allophycocyanin, clone N418; OX-6 anti-RT1.B, cross-reactive with H2-A$^{g7}$, unconjugated and FITC-conjugated; anti–H2-A$^{d/g7}$ (A$^{d/g7}$)–Alexa Fluor 647, clone 39-10-8; rat IgG2b-PE, clone RTK 530; and IgG3–Alexa Fluor 647 isotype control, clone MG3-35.

### Cell isolation and flow cytometry

Spleens were disrupted mechanically after enzymatic dissociation with Liberase CI (Roche), following the manufacturer's instructions. After incubation in mouse FcR blocking Reagent (Miltenyi Biotec), CD11c$^+$ and B220$^+$ cells were sequentially isolated by immunomagnetic labeling with CD11c and CD45R(B220) MACS MicroBeads (Miltenyi Biotec) and double-positive selection using an AutoMACS magnetic cell sorter (Miltenyi Biotec), following the manufacturer's instructions. Cell isolations were monitored by staining aliquots with fluorochrome–Ab conjugates against CD11c, CD19, and MHCII or isotype controls. Analysis was performed using a FACSCanto II flow cytometer (BD Biosciences) and FlowJo software (TreeStar). B cells and DCs were enumerated as CD19$^+$MHCII$^+$ and CD11c$^+$MHCII$^+$, respectively, after gating on intact splenocytes by forward and side scatter. MHCII and CD86 levels (median fluorescence intensities) were quantified after gating on cells expressing the appropriate lineage Ag within the scatter gate. Purified cell samples were washed in PBS, counted, and stored as pellets at $-20°$C.

### Protein isolation

Cell pellets were extracted in ice-cold TBS (pH 7.4) containing 1% IGEPAL CA-630 (Sigma) and protease inhibitors (Complete; Roche; plus 10 mM iodoacetamide). Extracts were centrifuged at $10,000 \times g$ to pellet nuclei and debris (stored at $-20°$C for subsequent DNA analysis, see below), and the supernatants were precleared and immunoprecipitated with appropriate anti-MHCII or isotype-control mAbs, as previously described (31). Immunoprecipitates were resolved by SDS-PAGE on hand-cast (12% acrylamide) or precast gels (Criterion TGX; Bio-Rad) under nonreducing conditions. Following silver staining, gel images were acquired using an EPSON Perfection 1650 flatbed scanner with Microsoft Scanner and Camera Wizard (default settings). Bands of interest were identified by comparison with control immunoprecipitates, excised, and stored at $-80°$C. In-gel reduction, derivatization of cysteines with iodoacetamide, and tryptic digestion were performed as previously described (31).

### Peptide liquid chromatography/mass spectrometry and calculation of protein fractional synthesis

Tryptic digests were analyzed by liquid chromatography/mass spectrometry (LC/MS), as previously described (31), except that an LTQ Orbitrap Velos tandem mass spectrometer (Thermo Scientific, San Jose, CA) was used. Data were acquired in data-dependent acquisition mode. Mass spectra of intact doubly charged or triply charged peptide ions were acquired in the Orbitrap detector set to 7500 resolution (defined at $m/z = 400$). Systematic error in mass isotopomer distributions is minimized at this resolution (R. Busch, M.F. Usmani, P.D. Charles, and M.J. Deery, unpublished observations) (41, 42). Tandem mass spectrometry (MS) data were acquired after collision-induced dissociation of the five most abundant peptides in each MS scan. Murine MHCII protein–derived peptides were identified using the Mascot search algorithm, with a mass tolerance of 25 ppm, carboxamidomethylation of cysteines as a fixed modification, and methionine oxidation as a variable modification.

For quantification of fractional protein synthesis ($f$), mass isotopomer distributions of unlabeled and labeled peptides of interest were obtained by integration of peptide ion chromatograms for the monoisotopic base peak ($m_0$) and higher mass isotopomers up to $m_2$ or $m_3$, as described previously (31). Fractional molar abundances were calculated by normalization to the total abundance in the mass envelope and compared with theoretical models, which were calculated by mass isotopomer distribution analysis (MIDA) (43), as implemented in Microsoft Excel (R. Busch, unpublished work; available on request). Mass isotopomer distributions progressively deviated from the unlabeled baseline during $^2$H$_2$O labeling, reaching a plateau after $\geq 10$ d. The maximal (plateau) shifts from the baseline were modeled by MIDA, using the measured body water enrichment to represent the precursor pool enrichment and adjusting the number of biosynthetic $^2$H-incorporation sites ($n$) to minimize the root-mean-square deviation between model and data. Fractional protein synthesis was calculated as the percentage of the maximal possible shift of each mass isotopomer from baseline (31). The calculations were adjusted for variations in $^2$H$_2$O enrichment between mice. Analytical error for each peptide was estimated as an SD of two or three informative mass isotopomers and was routinely <6%, except where mentioned. Summary estimates of fractional protein synthesis

were derived by averaging data from all available peptides (at least two), with an overall SD < 6%. Data points with greater analytical errors, in most cases due to low peptide ion abundance, were excluded.

### DNA processing and calculation of fractional cell turnover

DNA processing and calculation of fractional cell turnover was done as described (35), with minor modifications. Briefly, DNA-containing pellets from extracted cell samples (see above) were boiled in deionized water, undissolved material was removed by centrifugation, and the supernatant was subjected to DNA hydrolysis, mild acid release of deoxyribose from purine nucleotides, and chemical modification with pentafluorobenzyl hydroxylamine and acetic anhydride to generate the pentafluorobenzyl triacetyl derivative. The derivative was extracted with dichloromethane, dried overnight in vacuo, suspended in ethyl acetate, and injected in duplicate into a benchtop gas chromatograph/mass spectrometer (Hewlett-Packard). Measurements were performed in negative chemical ionization mode, with selected ion monitoring of the ion formed by loss of HF from the derivative, with $m/z$ 435 ($m_0$) or 436 ($m_1$). The fractional molar abundance of the $m_1$ mass isotopomer [= $m_1/(m_0+m_1)$] was calculated for all samples by integration of the major peak, representing the *trans* isomer of the derivative, in extracted ion chromatograms, using a previously described algorithm (44) in a MatLab implementation (M.C. Varley, unpublished observations). Unlabeled deoxyribose standards spanning the abundance range of samples were run, and abundance-corrected baseline values (35) were subtracted to generate excess $m_1$ (Em$_1$) values. Bone marrow harvested from femurs after $\geq 10$ d of $^2$H$_2$O labeling of mice was used as a fully labeled control. Em$_1$ values for unlabeled and fully labeled deoxyribose conformed closely to those observed in previous work (35), and duplicate measurements of Em$_1$ were routinely within 0.2% of the mean. Fractional DNA synthesis was calculated as $f_{cell} = $ (Em$_{1[sample]}$/Em$_{1[BM]}$), where [BM] refers to the average of Em$_1$ values for fully labeled bone marrow.

### Analysis of $^2$H$_2$O enrichment

Sera and media were diluted gravimetrically, and $^2$H$_2$O enrichment was quantified by isotope ratio MS, as previously described (31).

### Statistics

Statistical analysis was performed using GraphPad Prism software. Means and SD of data pooled from at least two independent labeling experiments were used as descriptive statistics. Strain differences in immunophenotypes were evaluated by unpaired, two-tailed Student $t$ test. Variation between peptides from the same protein sample was analyzed by one-way ANOVA. Two-way ANOVA was used to analyze the effects of cell lineage (B cell or DC) and either molecules/strains (A$^{g7}$ in NOD versus H2-A$^d$ [A$^d$] in BALB/c versus H2-E$^d$ [E$^d$] in BALB/c) or sex of NOD mice. The time course of $f$ was modeled for each molecule or cell population as either a single-exponential rise to maximum [$f(t) = 1 - e^{-kt}$], with rate constant $k$ and $t_{1/2} = \ln(2)/k$ or as the sum of two single-exponential terms, with rate constants $k_1$ and $k_2$, weighted in relative proportions w$_1$ and w$_2$ [$f(t) = w_1(1 - e^{-k1t}) + w_2(1 - e^{-k2t})$], by nonlinear least-squares fit to the data. Best-fit half-lives were reported with 95% confidence intervals. Curve fits using alternative models were compared using the F test. In addition, the F test was used to compare single-exponential half-lives between different molecules/strains or sexes. Kaplan–Meier analysis of cumulative disease incidence was performed, and incidence curves were compared by the log-rank test.

## Results

### Use of SINEW for measurement of MHCII protein turnover in vivo

We used the recently developed SINEW approach to address the role of MHCII turnover in NOD autoimmunity in vivo (31). SINEW uses MS to quantify the relative abundances of peptide mass variants ("mass isotopomers", differing by $\geq 1$ Da as the result of the presence of stable isotopes of any element at any position in the peptide). The resultant mass isotopomer distributions change upon $^2$H incorporation into proteins during continuous biosynthetic labeling with heavy water ($^2$H$_2$O), in proportion to the cumulative fraction of old molecules that has been replaced by new ones during the labeling interval (31). This measure, also known as fractional protein synthesis, equals protein turnover, provided that cell turnover is

negligible and levels of proteins of interest remain at steady state (Fig. 1A); these assumptions are tested further below.

The experimental design is summarized in Fig. 1B; steps a–d represent the measurement of fractional protein synthesis. Six-week-old female, prediabetic NOD and control mice (BALB/c: H2-A$^d$ and -E$^d$) were labeled in vivo with $^2H_2O$ for several weeks (Fig. 1B, step a). $^2H$ enrichments in body water were kept at ~4–5% throughout the labeling period, as verified by MS analysis of sera (Fig. 1C, data not shown).

Animals were sacrificed after various times; splenocytes were dissociated enzymatically and used for sequential MACS isolation of DCs (CD11c$^+$) and B cells (B220$^+$; Fig. 1B, step b). Flow cytometric enumeration of APCs before MACS enrichment revealed strain differences in APC composition (Fig. 2A–C). Spleens of young NOD females contained significantly greater proportions and absolute numbers of DCs, smaller proportions of B cells, and, thus, a higher ratio of DCs/B cells than were found in age- and sex-matched BALB/c mice. This was consistent with previous reports of lymphopenia and abnormal B cell development in NOD mice (45, 46). Despite these differences, DCs and B cells from both strains were successfully enriched to >90% purity by MACS (Fig. 2D, 2E). Indeed, >95% of MHCII$^+$ cells were of the desired lineage after enrichment (Fig. 2D, data not shown).

Next, MHCII molecules were immunoprecipitated from detergent extracts of APCs, using allele-specific mAbs (Fig. 1B, step c). MHCII α− and β-chains were separated by nonreducing SDS-PAGE and excised following silver staining (Fig. 3A). Tryptic digests were used for peptide mapping by tandem MS, which confirmed the presence of the MHCII molecules of interest (Fig. 3B). Mass isotopomer distributions of selected peptides were then quantified by LC/MS (31). An example is shown in Fig. 4A. The mass heterogeneity at baseline is largely explained by the random incorporation of [$^{13}C$] (~1.09% of total carbon in nature), with smaller contributions from other stable isotopes, which are less abundant in nature. During $^2H_2O$

labeling, $^2H$ incorporation shifted this baseline distribution toward heavier species, until a plateau was reached after ≥10 d of labeling, representing complete turnover of MHCII proteins. Both the unlabeled and fully labeled mass isotopomer distributions corresponded closely to theoretical predictions (Fig. 4A; see Refs. 31, 43 for details of the MIDA algorithms used). Informative peptides were selected for each of the MHCII molecules of interest, based on their total ion abundance, absence of peak contamination, agreement with MIDA predictions, and the magnitude of the shifts in the mass isotopomer distributions following $^2H_2O$ labeling. The peptides are shown in bold type in Fig. 3B; their mass isotopomer distributions and labeling statistics are summarized in the supplemental material (Supplemental Fig. 1, Supplemental Table I).

Previous work showed that, in partially labeled mass isotopomer distributions of peptides, the abundance of each individual mass variant is intermediate between unlabeled and fully labeled distributions, in proportion to the fractional synthesis of the protein of origin (31). On this basis, fractional synthesis values were calculated from multiple MHCII-derived peptides. Fig. 4B shows an analysis of B cells from individual mice labeled for 4 h. Within error, analysis of different peptides from the same MHCII molecule gave indistinguishable estimates of fractional protein synthesis (Fig. 4B). Subsequently, at least two informative peptides in each sample were analyzed, and fractional protein synthesis values were averaged (SD ≤ 6%).

### Effect of cell lineage on the turnover of different MHCII molecules in inbred mice

Fig. 4C summarizes the fractional synthesis of E$^d$, A$^d$, and A$^{g7}$ at 4 h for B cells, as well as DCs. Strikingly, all three MHCII molecules turned over much more actively in DCs than in B cells (Fig. 4C); these differences were more pronounced than those between MHCII molecules. Moreover, the allelic differences also depended on the APC type: in DCs, A$^{g7}$ had higher turnover than E$^d$ or A$^d$,



FIGURE 1. Measurement of MHCII turnover in vivo by SINEW. (**A**) Fractional protein synthesis, measured by SINEW, includes potential contributions from protein turnover, net protein synthesis, and cell proliferation. The latter contributions can be corrected for by quantifying steady-state protein levels and fractional DNA synthesis or neglected if they are small. (**B**) Work flow for measurements of fractional MHCII protein and DNA synthesis in APC populations of $^2H_2O$-labeled living mice. See text for details. (**C**) Equivalent $^2H_2O$ labeling of NOD and BALB/c mice. $^2H_2O$ a.p.e. was measured by isotope ratio MS in serum from 6-wk-old female BALB/c (n = 15) and NOD (n = 16) mice after up to 24 h of $^2H_2O$ labeling. There was no significant difference in average $^2H_2O$ labeling between strains (p > 0.05, Student t test). Serum $^2H_2O$ enrichments after 24 h (data not shown) were similar, on average, but less variable than at the earlier time points.
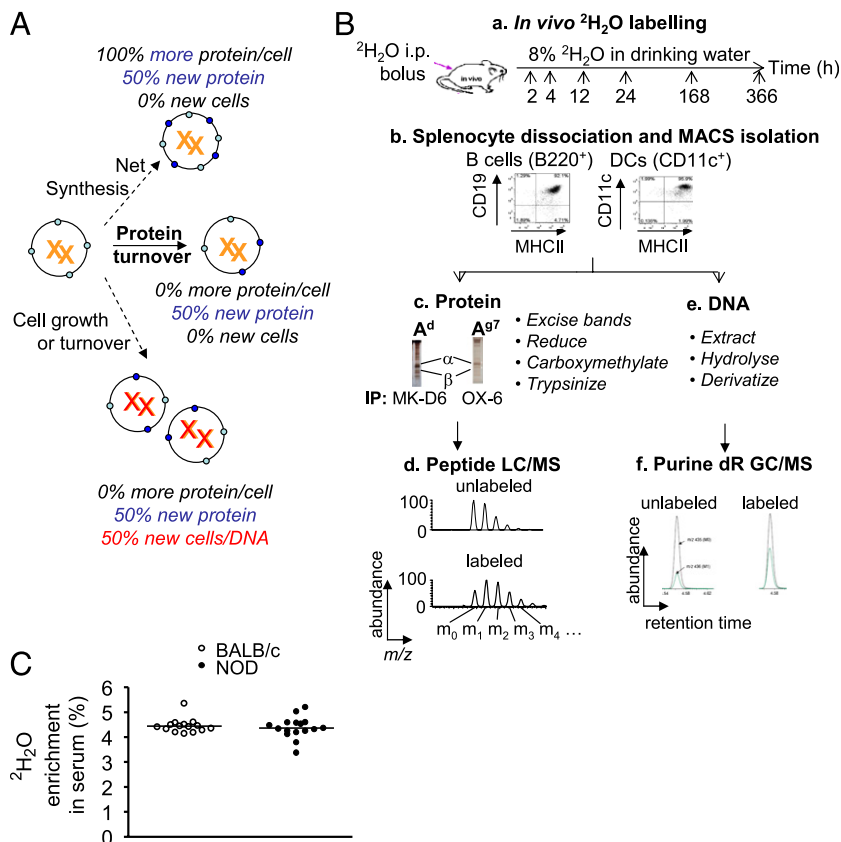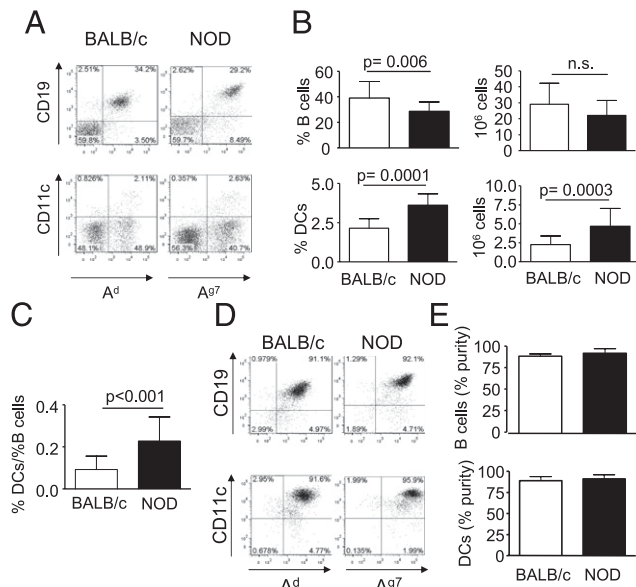
**FIGURE 2.** Purification of splenic APC populations from $^2H_2O$-labeled NOD and BALB/c mice. (**A** and **B**) Flow cytometric analysis of enzymatically dissociated whole splenocytes for MHCII and lineage markers of either B cells (CD19; *upper panels*) or DCs (CD11c; *lower panels*). Representative dot plots (A), percentages (B, *left panels*), and absolute cell counts (B, *right panels*) are shown (mean ± SD, $n = 16$/strain; $p$ values by Student $t$ test). (**C**) Ratio of percentage of splenic DCs/splenic B cells (BALB/c, $n = 21$; NOD, $n = 17$; $p$ value by Student $t$ test). (**D** and **E**) Purity of MACS-enriched APC populations. Sequential AutoMACS isolation of splenic B220$^+$ B cells (*upper panels*) and CD11c$^+$ DCs (*lower panels*) was monitored. Representative dot plots (D) and percentages (E) of enriched populations are shown. Purity was routinely >90% lin$^+$ H2-A$^+$ (*right panels*), and >95% of H2-A$^+$ cells were of desired lineage. Spleens were obtained from female NOD ($n = 16$) and BALB/c ($n = 15$) mice, aged 5–6 wk, and labeled for up to 24 h. Similar data were obtained after extended $^2H_2O$ labeling (data not shown).

but in B cells, E$^d$ turnover was similar to A$^{g7}$ and faster than A$^d$. We concluded that structural polymorphism is not the sole determinant of MHCII turnover in vivo, whereas the cell lineage is a major determinant.

When tracked over time, MHCII protein fractional synthesis in B cells increased continuously, approaching 100% replacement of old molecules within a week (Fig. 5A, 5B; statistics are summarized in Fig. 5C). Single-exponential curve fits indicated average fractional synthesis $t_{1/2}$ ~10–12.5 h. Consistent with data obtained at 4 h, the half-lives for A$^{g7}$ and E$^d$ were slightly, but significantly, shorter than for A$^d$ (Fig. 5C; compared by F test). Interestingly, however, data for A$^{g7}$ turnover deviated significantly from a single-exponential model with a uniform half-life (by Runs test) and were significantly better modeled by a mixture of fast- and slow-turnover subpopulations (Fig. 5B, 5C). The fast phase explained the difference between A$^d$ and A$^{g7}$ at 4 h, which disappeared later in the experiment. Thus, fast turnover appears to be characteristic of only a fraction of A$^{g7}$ molecules.

In contrast, turnover of A$^{g7}$ in M12 B lymphoma transfectants labeled in vitro was uniformly slow, without evidence of a fast phase (Supplemental Fig. 2) (31). Thus, the presence of kinetic heterogeneity seemed to depend on the cellular context.

*Fractional synthesis is a measure of MHCII protein turnover in vivo*

In addition to the need to replace turned-over protein, another reason for the synthesis of new cell-associated molecules could be
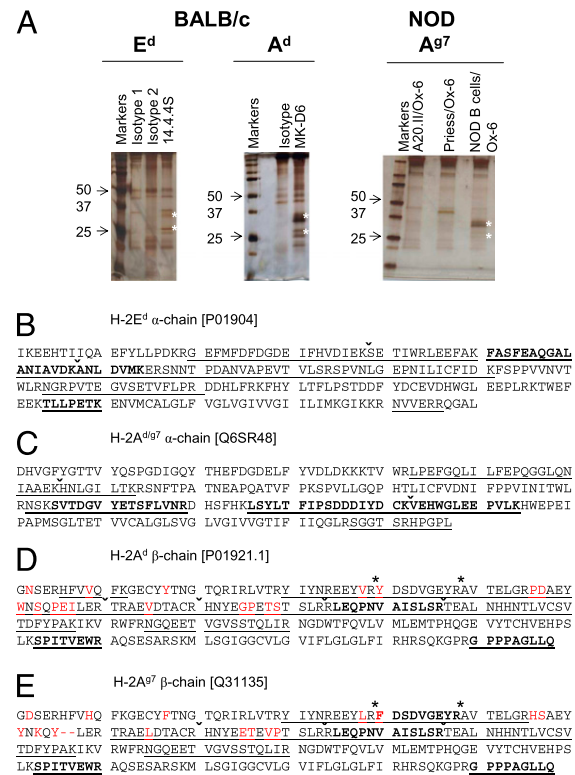
**FIGURE 3.** Isolation and peptide mapping of MHCII molecules. (**A**) MHCII molecules were immunoprecipitated with 14-4-4S, IgG2a anti–H2-E$^d$ (*left panel*), MK-D6, IgG2a anti–H2-A$^d$ (*center panel*), and OX-6, IgG1 anti–H2-A$^{g7}$ (*right panel*) and either protein A– or protein G–Sepharose from BALB/c or NOD splenic B cells (2–3 × 10$^7$), resolved by SDS-PAGE under nonreducing conditions, and visualized by silver staining. MHCII α- and β-chain bands (*) were identified by comparison with controls (isotype-matched irrelevant Ab) or irrelevant cells (A20, mouse B lymphoma line; Priess, human B-lymphoblastoid line) and excised for tryptic peptide mapping. Note that, although both chains of the αβ heterodimer are present in equimolar amounts, the H2-Aα-chain stained better with silver. Each panel represents an independently acquired gel image. (**B–E**) Tryptic peptide mapping. Bands of interest from (A) were digested with trypsin and analyzed by tandem MS, and peptides were identified by database searches. Amino acid sequences of mature E$^d$ α-chain (B), A$^{d/g7}$ α-chain (C), A$^d$ β-chain (D), and A$^{g7}$ β-chain (E) were obtained from the Uniprot database (accession numbers are shown in brackets) and given in single-letter code. Underlined tryptic fragments were detected by tandem MS. The symbols ˇ and * indicate positions of complete and partial cleavage sites, respectively, where not evident from underlining. Structural polymorphisms distinguishing A$^d$ and A$^{g7}$ β-chains are shown in red; dashes indicate amino acid deletion. Peptides shown in bold were used for measurements of fractional protein synthesis.

**B** H-2E$^d$ α-chain [P01904]

```
IKEEHTIIQA EFYLLPDKRG EFMFDFDGDE IFHVDIEKSE TIWRLEEFAK FASFEAQGAL
ANIAVDKANL DVMKERSNNT PDANVAPEVT VLSRSPVNLG EPNILICFID KFSPPVVNVT
WLRNGRPVTE GVSETVFLPR DDHLFRKFHY LTFLPSTDDF YDCEVDHWGL EEPLRKTWEF
EEKTLLPETK ENVMCALGLF VGLVGIVVGI ILIMKGIKKR NVVERRQGAL
```

**C** H-2A$^{d/g7}$ α-chain [Q6SR48]

```
DHVGFYGTTV YQSPGDIGQY THEFDGDELF YVDLDKKKTV WRLPEFGQLI LFEPQGGLQN
IAAEKHNLGI LTKRSNFTPA TNEAPQATVF PKSPVLLGQP HTLICFVDNI FPPVINITWL
RNSKSVTDGV YETSFLVNRD HSFHKLSYLT FIPSDDDIYD CKVEHWGLEE PVLKHWEPEI
PAPMSGLTET VVCALGLSVG LVGIVVGTIF IIQGLRSGGT SRHPGPL
```

**D** H-2A$^d$ β-chain [P01921.1]

```
GNSERHFVVQ FKGECYYTNG TQRIRLVTRY IYNREEYVRY DSDVGEYRAV TELGRPDAEY
WNSQPEILER TRAEVDTACR HNYEGPETST SLRRLEQPNV AISLSRTEAL NHHNTLVCSV
TDFYPAKIKV RWFRNGQEET VGVSSTQLIR NGDWTFQVLV MLEMTPHQGE VYTCHVEHPS
LKSPITVEWR AQSESARSKM LSGIGGCVLG VIFLGLGLFI RHRSQKGPRG PPPAGLLQ
```

**E** H-2A$^{g7}$ β-chain [Q31135]

```
GDSERHFVHQ FKGECYFTNG TQRIRLVTRY IYNREEYLRF DSDVGEYRAV TELGRHSAEY
YNKQY--LER TRAELDTACR HNYEETEVPT SLRRLEQPNV AISLSRTEAL NHHNTLVCSV
TDFYPAKIKV RWFRNGQEET VGVSSTQLIR NGDWTFQVLV MLEMTPHQGE VYTCHVEHPS
LKSPITVEWR AQSESARSKM LSGIGGCVLG VIFLGLGLFI RHRSQKGPRG PPPAGLLQ
```

the requirement to maintain steady-state protein levels as cells divide (Fig. 1A). To assess whether cell division contributed substantially to the need for MHCII protein synthesis, fractional DNA synthesis was quantified by $^2H_2O$ labeling, using previously established, well-validated methods (Fig. 1B, steps e and f) (35). As expected, B cell proliferation occurred on much slower time scales ($t_{1/2}$ ~2 wk) than did MHCII fractional synthesis (Fig. 5A, 5B). DC renewal was faster (data not shown), but it did not contribute substantially to protein synthesis at early time points (≤3% new cells at 4 h). Thus, proliferative cell renewal did not contribute substantially to the observed rates of MHCII fractional synthesis in vivo. In contrast, A$^{g7}$ fractional protein synthesis in the M12 B lymphoma line was entirely attributable to cell growth, with no detectable additional contribution from protein turnover
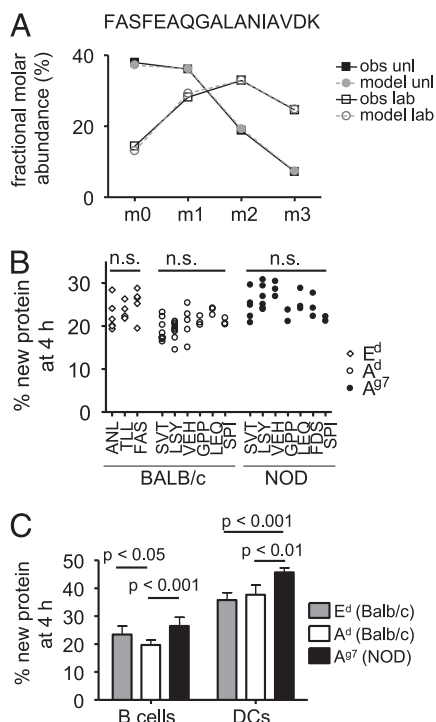
**FIGURE 4.** Measurement of fractional MHCII protein synthesis and comparison in B cells and DCs after 4 h of in vivo labeling. (**A**) Mass isotopomer distributions of a typical peptide from $E^d$ α-chain are shown, by way of example, at baseline ("unl") and after labeling of BALB/c mice to plateau (14 d; "lab"). Predicted distributions ("model") were obtained by MIDA calculations and compared with measurements by LC/MS ("obs"). The mass variant (mass isotopomer) containing only the lightest isotopes of each element is designated "m0"; m1, m2, and m3 have 1, 2, or 3 extra Da from incorporation of one or more heavier isotopes of any element. The fractional molar abundance of each mass isotopomer is shown. Fractional synthesis in partially labeled samples is calculated by interpolation between the unlabeled and fully labeled distribution, averaged across all informative mass isotopomers. (**B**) Indistinguishable estimates of fractional synthesis obtained by analysis of different peptides from the same MHCII protein. Fractional MHCII protein synthesis was quantified in B cells isolated after 4 h of $^2H_2O$ labeling in vivo. Data are shown for different peptides (identified by the first three amino acids in each sequence; compare with Fig. 3B) from individual animals. Data were pooled from at least two independent labeling experiments for each strain. Fractional synthesis estimates from different tryptic fragments of the same protein were statistically indistinguishable ($p > 0.05$, one-way ANOVA). (**C**) APC lineage and mouse strain affect MHCII turnover at 4 h in vivo. The fraction of new MHCII molecules is shown after 4 h of $^2H_2O$ labeling of female, 4–6-wk-old mice. Mean ± SD are shown for splenic $B220^+$ B cells from eight ($E^d$) or nine ($A^d$) individual BALB/c mice and five NOD mice, as well as for $CD11c^+$ DCs from five BALB/c mice and two independently labeled pools of three NOD mice. Fractional synthesis was averaged from two or three mass isotopomers of two to seven MHCII-derived peptides/animal. Data from at least two independent labeling experiments/group were pooled. Effects of APC lineage ($p < 0.0001$) and molecules/strains ($p < 0.0001$) on turnover, as well as their mutual interaction (i.e., the hierarchy of molecules depends on the cell type: $p = 0.0175$), were significant (two-way ANOVA). The $p$ values in the Figure show significant differences between molecules within each cell lineage (Bonferroni posttest). n.s., Not significant.

(Supplemental Fig. 2). We estimated that the half-life for $A^{g7}$ turnover was ≥42 h in this cell line.

In addition, we considered the possibility that a proportion of splenic B cells might be activated in NOD B cells and that this might contribute to heterogeneous $A^{g7}$ turnover (47). As a positive control, upregulation of MHCII, CD86, and other activation markers
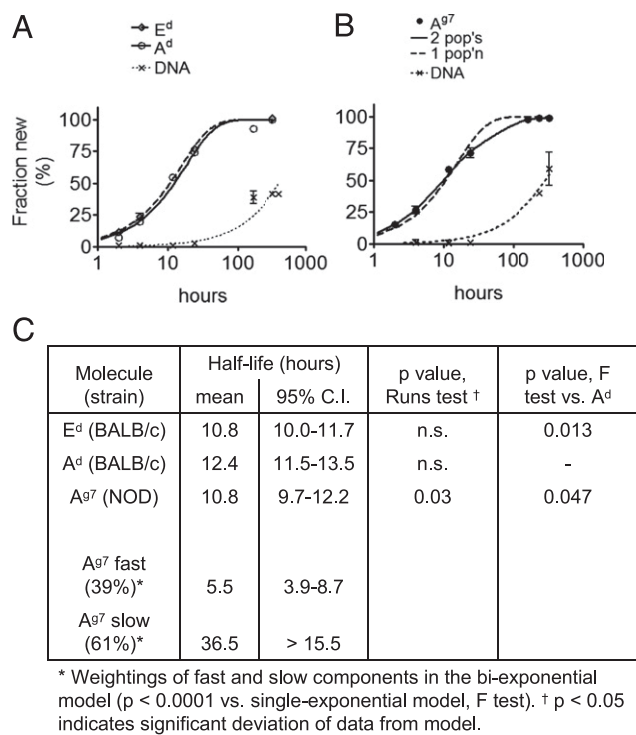


**FIGURE 5.** Time course of MHCII protein fractional synthesis and DNA turnover in B cells. (**A**) Fractional synthesis of H2-$A^d$ and $E^d$ and of DNA (cell turnover) in BALB/c B cells over time. Note log scale for labeling times. Symbols represent mean ± SD fractional synthesis from 1–9 animals/time point (protein data from 19 mice in total analyzed for $A^d$ and 14 mice for $E^d$, pooled from two independent experiments). Lines are single-exponential curve fits. Cell turnover was slow ($t_{1/2} \sim 420$ h). (**B**) Fractional synthesis of $A^{g7}$ and DNA in NOD B cells over time. Analysis as in (A) ($n = 20$ mice, pooled from two independent experiments). Mono- and biexponential (two-population) curve fits are shown. Cell turnover was slow ($t_{1/2} \sim 290$ h). (**C**) Kinetic parameters and statistics for the curve fits in (A) and (B).

| Molecule (strain) | Half-life (hours) mean | Half-life (hours) 95% C.I. | p value, Runs test † | p value, F test vs. $A^d$ |
|---|---|---|---|---|
| $E^d$ (BALB/c) | 10.8 | 10.0-11.7 | n.s. | 0.013 |
| $A^d$ (BALB/c) | 12.4 | 11.5-13.5 | n.s. | - |
| $A^{g7}$ (NOD) | 10.8 | 9.7-12.2 | 0.03 | 0.047 |
| $A^{g7}$ fast (39%)* | 5.5 | 3.9-8.7 | | |
| $A^{g7}$ slow (61%)* | 36.5 | > 15.5 | | |

\* Weightings of fast and slow components in the bi-exponential model ($p < 0.0001$ vs. single-exponential model, F test). † $p < 0.05$ indicates significant deviation of data from model.

was readily detected on B cells stimulated in vitro with LPS over a wide dose range (data not shown). However, flow cytometric analysis of MHCII (Fig. 6A, 6B) and CD86 (Fig. 6C, 6D) ex vivo showed no evidence of B cell activation or heterogeneous MHCII expression. In addition, these experiments showed no evidence of inadvertent activation of APCs in vivo due to the i.p. bolus injection of $^2H_2O$ used to initiate labeling. Pilot experiments revealed the presence of low levels of LPS in some batches of $^2H_2O$, which were sufficient to cause slight activation of APCs in vitro (A. De Riva, unpublished observations). To avoid the possibility that LPS activation could confound the turnover measurements, LPS was routinely removed from $^2H_2O$ preparations used for i.p. bolus injection. Lastly, there was no evidence for changes in MHCII levels over the course of the labeling experiments (Fig. 6A, 6B, data not shown), arguing against the possibility that some of the measured new synthesis might be attributable to net accumulation of new MHCII molecules (Fig. 1A). Taken together, these additional controls showed that changes in MHCII levels and cell proliferation did not contribute markedly to fractional MHCII protein synthesis, implying that fractional synthesis is equivalent to protein turnover in this system (Fig. 1A).

*Biological variables affecting the accelerated turnover of $A^{g7}$ molecules in NOD mice*

Further experiments were undertaken to identify determinants of the difference in turnover between H2-$A^d$ in BALB/c B cells and

**FIGURE 6.** $^2H_2O$ labeling does not perturb MHCII or CD86 expression. (**A** and **B**) Analysis of MHCII surface levels. Representative flow cytometry graphs (A) and median fluorescence intensities (MFI) (B) of $A^d$ (MK-D6) and $A^{g7}$ (OX-6) levels on gated splenic B220$^+$ B cells (*left panels*) or CD11c$^+$ DCs (*right panels*) from five BALB/c mice (*top panels*) and six NOD mice (*bottom panels*) given $^2H_2O$ (+) and two NOD mice and one BALB/c mouse given natural-abundance saline (-), sacrificed up to 24 h post-injection. $^2H_2O$ labeling had no effect ($p > 0.05$, t test). Isotype control MFI values averaged ~100 in both strains. Results are representative of all experiments, at all time points. (**C** and **D**) Analysis of CD86 levels. Representative flow cytometry graphs (C) and MFIs (D; mean ± SD) showing CD86 staining of mock-injected or $^2H_2O$-labeled splenic CD19$^+$ B cells or CD11c$^+$ DCs from BALB/c or NOD mice. Numbers of animals were as in (B). Negative controls in (C) were gated on CD3$^+$ cells. Splenocytes from the two strains were stained on different days, so that MFI values are not directly comparable between strains. CD86 levels were monitored in all experiments, and the lack of $^2H_2O$ effect was consistent throughout.
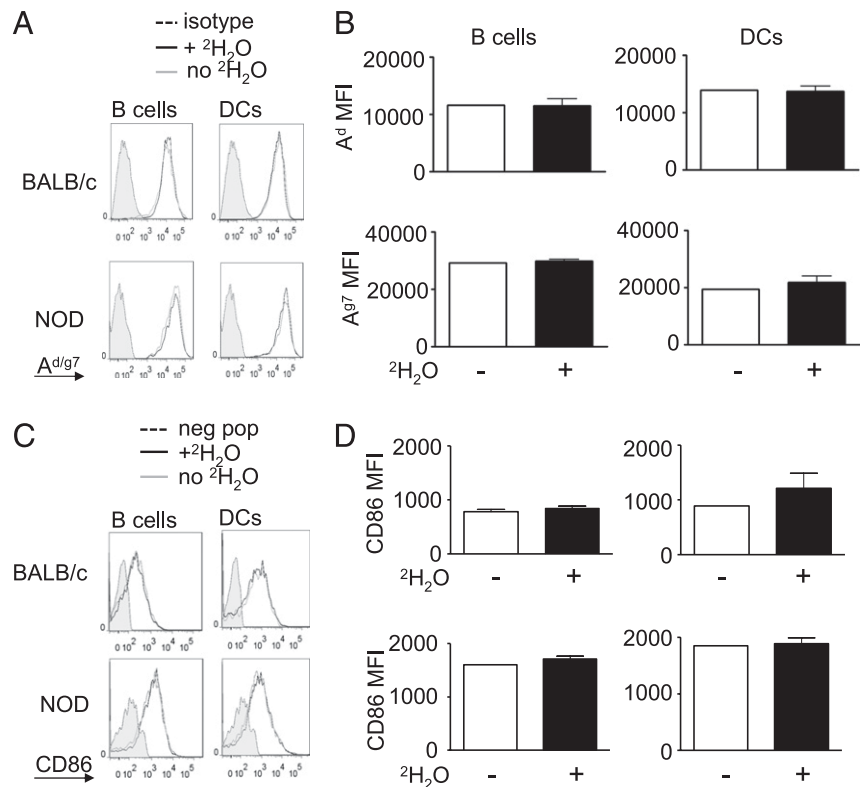
$A^{g7}$ in NOD B cells at early time points. If this difference reflects an inherent structural defect of $A^{g7}$, then it should be detectable in (NOD × BALB/c) F1 mice. However, $A^d$ and $A^{g7}$ isolated from F1 B cells showed equal turnover at 4 h (Fig. 7A). The two molecules were not mutually contaminated, as judged by analysis of tryptic digests (Supplemental Table II); F1 B cells were highly pure and not activated, as judged by analysis of MHCII and CD86 expression (Fig. 7B–D). Thus, the turnover difference between $A^d$ and $A^{g7}$ in the parental strains is not determined by the allelic difference but by the context in which the H2-A molecules is expressed.

In contrast, developmental variables affected $A^{g7}$ turnover in NOD B cells. Turnover was indistinguishable between males and females, both at 4 h and in B cells over time (Fig. 8A, 8B), but it declined by 12 wk of age to rates similar to $A^d$ turnover in young BALB/c mice (Fig. 8C).

To address the role of environmental variables in the regulation of MHCII turnover, $A^{g7}$ turnover at 4 h in splenic B cells from young female mice was compared between two NOD colonies housed in different animal facilities (Fig. 9). In the colony used for the previous experiments, ~22% of females developed T1D by 30 wk of age, which is at the low end of the range of disease penetrance observed worldwide ("NOD$^{low}$", Fig. 9A) (26). In contrast, as many as 91% of the females in the second ("NOD$^{high}$") colony developed diabetes. Unlike the NOD$^{low}$ colony, $A^{g7}$ in B cells from young female NOD$^{high}$ animals showed no evidence of accelerated turnover at the informative 4-h time point (Fig. 9B). The purity of MACS-enriched NOD$^{high}$ B cells (Fig. 9C), their non-activated phenotype (Fig. 9D, 9E), and B cell subset composition (data not shown) were similar to NOD$^{low}$ animals (Fig. 6). Together, these data show that environmental differences affect $A^{g7}$ turnover in apparently nonactivated B cells. Interestingly, $A^{g7}$ turnover was not accelerated in the high-incidence colony (Fig. 9A, 9B), indicating that accelerated turnover was dispensable for the development of T1D.

## Discussion

To our knowledge, this study reports the first measurements of MHCII protein turnover in living mice. Moreover, this study provides evidence against the hypothesis that an intrinsic stability defect in $A^{g7}$ contributes to the pathogenesis of autoimmune diabetes.

The SINEW approach, previously validated to measure MHC protein synthesis in cultured cell lines (31), was used in this study in vivo to compare the turnover rates of different MHCII molecules in NOD and control mice. The studies were carefully controlled to avoid perturbation of the system by LPS contamination during $^2H_2O$ label administration. There was no evidence for perturbation of APCs by $^2H_2O$ itself. Measurements of the proliferative renewal of APCs and of MHCII levels showed that protein turnover was the only significant contributor to MHCII fractional synthesis. In principle, cell turnover could be a confounding variable in measuring the turnover rates of long-lived, cell-associated proteins, yet this is rarely considered in kinetic proteomics experiments. The ability of $^2H_2O$ to label both newly synthesized proteins and DNA (the latter representing cell turnover) represents a distinct advantage of SINEW over SILAC. The SINEW measurements were analytically precise and accurate, as judged by the close agreement of data with MIDA predictions. The measurements were validated by analysis of multiple peptides from each MHCII molecule. SINEW relies on quantitative shifts in peptide mass isotopomer distributions following $^2H_2O$ labeling; these shifts are subtler than the larger mass shifts created in SILAC by use of all-[$^{13}C$]-labeled amino acids. Nonetheless, the analytical characteristics of the SINEW approach permitted small differences in MHCII protein turnover to be detected.

Key determinants of MHCII protein turnover in vivo were identified. APC type had a substantial effect. In DCs, the ~40% replacement of old by new molecules after 4 h of labeling corresponds to an average $t_{1/2}$ ~5–6 h, about twice as fast as that observed in B cells ($t_{1/2}$ ~10–12 h). These findings correlate with recent studies, showing that murine DCs have higher rates of
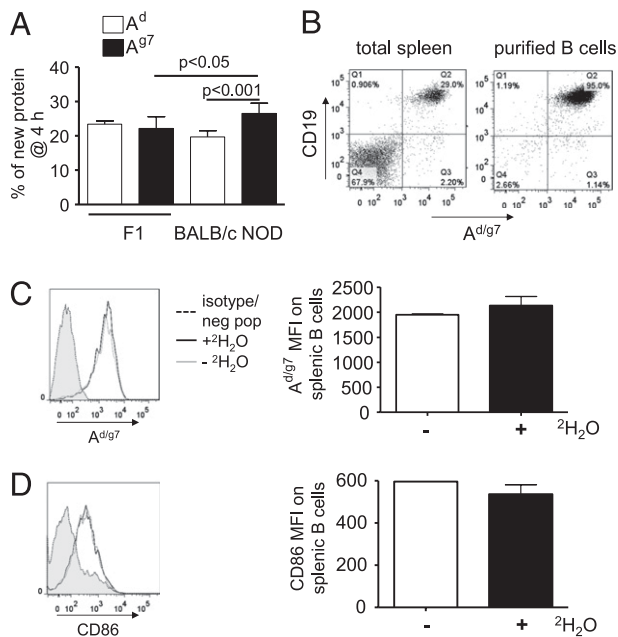
**FIGURE 7.** Indistinguishable turnover of $A^d$ and $A^{g7}$ in B cells from (BALB/c × NOD) F1 mice. (**A**) Fractional protein synthesis of $A^{g7}$ ($n = 5$ mice) and $A^d$ ($n = 4$ mice) at 4 h in splenic B cells of 6-wk-old female (BALB/c × NOD) F1 mice. Data were pooled from two independent experiments. Parental strains (from Fig. 4C) are shown for comparison. The $p$ values were calculated using one-way ANOVA. (**B**) B cell purity in the analyses shown in (A). Representative flow cytometry dot plots of CD19 versus H2-$A^{d/g7}$ expression (stained with the cross-reactive 39-10-8 mAb) on total splenocytes (*left panel*) and purified B cells (*right panel*). Lack of B cell activation in F1 mice, as assessed by flow cytometric analysis of MHCII (**C**) and CD86 (**D**) expression gated on CD19$^+$ B cells in total splenocytes. Representative flow cytometry graphs (*left panels*; dark line: $^2H_2O$-labeled; light line: natural-abundance control; filled graphs: negative controls). Isotype controls were used for class II stains in (C); negative control population for CD86 was gated on CD3$^+$ cells in (D). Median fluorescence intensities (mean ± SD) for six $^2H_2O$-injected F1 mice and one normal saline-injected control mouse (*right panels*). There was no evidence for phenotypic activation with or without $^2H_2O$.

ubiquitin-dependent MHCII internalization than do B cells in vitro (17); this is thought to regulate lysosomal degradation of MHCII molecules. MHCII turnover was much slower still ($t_{1/2} \geq 42$ h) in transfected M12 B lymphoma cells. Thus, some immortalized cell lines, which are useful in studying other aspects of Ag presentation, are poor models for studying the physiological regulation of MHCII protein turnover.

In B cells, the early kinetics of H2-A turnover measured by SINEW in vivo was comparable to the kinetics observed previously in vitro by pulse-chase analysis of unseparated splenocytes for up to 8 h (13). This was expected, given that B cells dominated quantitatively among splenic APCs in both mouse strains. However, possible confounding effects of APC composition must be considered when interpreting turnover measurements in whole splenocytes. We found that NOD spleens contain a higher ratio of DCs/B cells than do BALB/c spleens. Therefore, the higher MHCII turnover in DCs might have added to the differences in total splenic MHCII turnover between these strains, although model calculations suggest that this effect is not large (data not shown).

Conceivably, subpopulations within the DC or B cell lineage might also differ in MHCII protein life span. B cell subsets differ in their ubiquitin-dependent regulation of MHCII expression (47) and in their expression of DO, a regulator of DM-mediated peptide
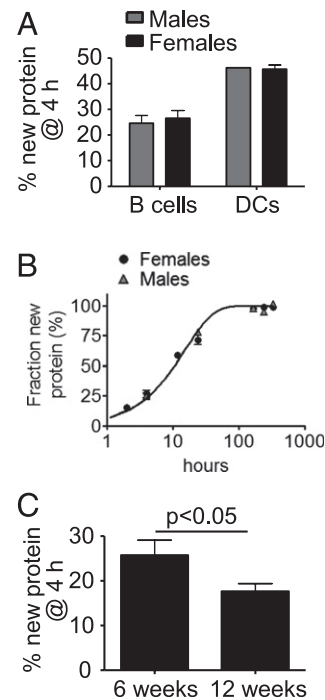


**FIGURE 8.** Sex and age effects on $A^{g7}$ turnover in NOD mice. (**A** and **B**) No sex effect on $A^{g7}$ fractional synthesis. (A) Analysis of B cells ($n = 3$) and DCs ($n = 1$) from male NOD mice at 4 h compared with females (reproduced from Fig. 4C). The effect of cell type was significant ($p < 0.0001$); the effect of sex was not significant ($p = 0.74$; two-way ANOVA). (B) Analysis of B cells over a labeling time course, as in Fig. 5. The best single-exponential curve fit ($t_{1/2} = 10.5$ h, 95% confidence interval: 9.4–11.9 h) was not significantly different from females ($p = 0.79$, F test). The data for males ($n = 9$ animals analyzed at five time points) were insufficient for a biexponential curve fit. (**C**) $A^{g7}$ turnover at 4 h in purified splenic B cells of 6-wk-old (from Fig. 2A) versus 12-wk-old ($n = 3$) female NOD mice. The $p$ value was calculated using the Student $t$ test.

exchange (23, 25). This could affect peptide loading, with possible implications for MHC protein stability (22). However, $A^d$- and $E^d$-labeling kinetics in BALB/c B cells conformed closely to a single-exponential curve fit, suggesting that the turnover rates of these molecules in the major B cell subsets are fairly uniform. Nonetheless, rare subsets could exhibit distinct rates of turnover.

In vitro, activation of APCs by proinflammatory stimuli is a major regulator of MHCII protein turnover. This is clearly evident in LPS- and cytokine-stimulated human and murine DCs, which, following an initial burst of MHCII synthesis, shut down ubiquitin-dependent MHCII internalization and degradation to enable persistent Ag presentation (19). The resultant shutdown in MHCII turnover is readily observed in vitro in LPS-stimulated human DCs by our SINEW approach (C. Prevosto, R. Busch, unpublished observations). In our studies, there was no evidence for activation of B cells or DCs in the spleens of $^2H_2O$-labeled mice when analyzed ex vivo; as a positive control, MHCII, CD86, and other activation markers were upregulated in splenic B cells stimulated with LPS in vitro (data not shown). We concluded that the MHCII turnover rates observed in vivo represent nonactivated conditions; the impact of APC activation will be an interesting direction of further research.

Compared with the large differences in MHCII turnover between APC types, the differences between MHCII molecules were less pronounced. In B cells and in DCs from inbred strains, initial measurements revealed slightly faster turnover rates for $A^{g7}$ than for $A^d$, reproducing the direction of trends observed previously
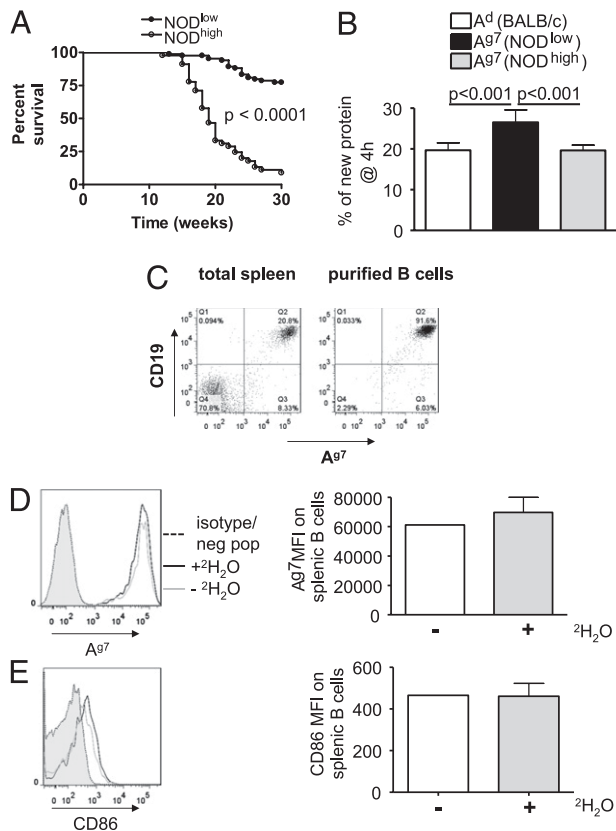
**FIGURE 9.** Lack of accelerated $A^{g7}$ turnover in B cells in a second colony of NOD mice with high T1D incidence. (**A**) Kaplan–Meier analysis of T1D incidence in female mice as a function of age in the NOD[low] ($n = 85$) versus the NOD[high] ($n = 45$) colony. The $p$ value was calculated using the log-rank test. (**B**) $A^{g7}$ turnover in splenic B cells at 4 h differs between 6-wk-old female mice from the NOD[low] and NOD[high] colonies. Data from NOD[high] mice ($n = 6$, pooled from two independent experiments) were compared with those for NOD[low] and BALB/c controls (from Fig. 4C) by one-way ANOVA. (**C**) Representative dot plot of CD19 versus MHCII expression in total splenocytes (*left panel*) and purified B cells (*right panel*). B cell activation was assessed by flow cytometric analysis of MHCII (**D**) and CD86 (**E**) expression after gating for CD19^{+} splenocytes. Representative flow cytometry graphs (*left panels*, dark line: $^2H_2O$; gray line: natural-abundance control; filled graphs: isotype controls/negative population, as in Fig. 7C, 7D). Median fluorescence intensities (*right panels*; mean ± SD) for six $^2H_2O$-injected NOD mice and one normal saline-injected NOD mouse. There was no evidence for phenotypic activation with or without $^2H_2O$.

in vitro (13). Albeit statistically significant and consistent within and between experiments, the difference was ~20% or less, whether it was measured at a single informative time point or in terms of average half-lives calculated from single-exponential curve fits. Moreover, in B cells, the turnover of protective H2-E molecules was indistinguishable from that of the $A^{g7}$ susceptibility allele. Thus, differences in overall turnover rates were minor and did not correlate with the contributions of different MHCII molecules to T1D risk. This is consistent with our serological studies (described above, and A. De Riva, unpublished observations), which provide no support for the notion that $A^{g7}$ is defective in surface expression compared with other MHCII alleles.

However, the time course data for NOD B cells revealed another possibility: they implied that $A^{g7}$ turnover rates are heterogeneous, with significant populations of both long-lived and short-lived molecules, compared with the uniform half-life of $A^d$. The clear difference between $A^d$ and $A^{g7}$ seen at early time points became

undetectable later in the experiment; a biexponential model fit the data better than did a model with uniform half-life. It was conceivable that this kinetic heterogeneity might have pathogenic significance. Therefore, further experiments were undertaken to characterize the fast-turnover $A^{g7}$ molecules. These studies focused on the 4-h time point, at which strain differences attributable to the fast-turnover kinetic component were clearly detectable.

Several observations indicated that the fast-turnover $A^{g7}$ subpopulation did not arise from an intrinsic stability defect of the $A^{g7}$ allele. First, an intrinsic defect would predict a uniformly fast rate of $A^{g7}$ turnover, but a single-exponential labeling curve with a short half-life was inconsistent with our data. Second, $A^d$ and $A^{g7}$ turnover were indistinguishable in B cells from H2[d×g7] F1 mice, showing that, in one and the same cellular environment, the 17-aa differences between these alleles have no detectable effect on turnover. Third, the turnover rate of $E^d$ was similar to that of $A^d$ in DCs, but it was similar to $A^{g7}$ in B cells, indicating that the cellular context influences relative turnover rates of different MHCII molecules. An overriding effect of the cellular microenvironment was indicated by the fact that the $A^{g7}$ molecules in the M12 B lymphoma transfectant were uniformly long-lived. Male and female NOD mice had similar $A^{g7}$ turnover; however, the accelerated turnover at 4 h was not observed in older NOD mice, and it was not present in B cells from a second colony of NOD mice housed under different environmental conditions. This responsiveness to developmental and environmental variables argued that $A^{g7}$ turnover is not determined by any intrinsic stability defect.

The environmental regulation of MHCII turnover contrasts with the marked influence of structural polymorphism on the SDS stability of different H2-A alleles, noted previously by other investigators (13). Our results imply that MHCII turnover rates and SDS stability may be discordantly regulated, so that SDS instability does not necessarily predict a shortened MHCII life span.

We considered the possibility that cellular heterogeneity could contribute to the kinetic heterogeneity of $A^{g7}$ molecules in NOD B cells. Preliminary experiments showed no difference in $A^{g7}$ turnover at 4 h between MACS-isolated total B220^{+} B cells and FACS-sorted follicular B cells (data not shown). Moreover, the difference in $A^{g7}$ turnover between the two colonies of NOD mice was not explained by differences in phenotypic activation of splenic B cells (which was undetectable in both colonies) or in their subset composition (data not shown). These experiments do not rule out cellular heterogeneity as a contributing variable. Alternatively, heterogeneous $A^{g7}$ turnover could arise from heterogeneous editing of the bound peptide repertoire. This possibility is difficult to address directly with our current methodology, which is not able to measure the turnover rates of specific peptide/MHCII protein complexes. Regardless of the underlying mechanisms, our data indicate that environmental and developmental factors modify the handling of MHCII molecules in splenic B cells, even in the absence of overt phenotypic activation.

Collectively, our studies argue strongly against a disease-promoting role for accelerated turnover in the mechanisms linking the $A^{g7}$ allele to T1D pathogenesis, which was postulated earlier (9, 13). As argued above, the complex dynamics of $A^{g7}$ turnover in NOD spleens was determined by environmental and developmental variables, rather than by MHCII polymorphism; thus, it did not offer a link between MHCII polymorphism and disease. It had only a small effect on average molecular life spans and no discernible effect on the steady-state expression of $A^{g7}$, limiting its potential impact on T cell tolerance. Most importantly, accelerated turnover of some $A^{g7}$ molecules in splenic B cells was observed only in a NOD colony with low T1D incidence and not

in a second colony with high disease incidence. Thus, the dynamic abnormality was not required for T1D development in this high-incidence NOD colony. The simplest explanation is that this phenotype represents an epiphenomenon in T1D pathogenesis.

Although these data argue strongly against a causal role for a generalized, inherent defect in $A^{g7}$ turnover, abnormalities in specialized niches could prove to be relevant to pathogenesis. This could include, for example, activated APCs in lesional tissue, which contribute to T1D pathogenesis from an early stage, and thymic APCs, which maintain central tolerance. The sample requirements of SINEW experiments have not permitted analyses of these less abundant populations. However, with regard to thymic APCs, we note recent work that suggests that central tolerance in NOD mice is not compromised by an Ag-presentation defect, but rather is overwhelmed by a surfeit of $\alpha\beta$ over $\gamma\delta$ T cell precursors during thymic development (48).

Independently of the question of whether $A^{g7}$ turnover contributes to T1D pathogenesis, the differences between the two NOD colonies raised important questions for future research. A key priority will be the isolation of specific environmental variables that determine the large differences in disease incidence. We excluded genetic contamination of the low-incidence colony. Differences in microbiological status, identified by veterinary and in-house screening (data not shown), did not involve species known to influence T1D incidence in NOD mice (27), and broader differences in microbiota and minor differences in husbandry practices could also contribute. A related question is how these environmental variables could influence the dynamics of $A^{g7}$ turnover in splenic B cells without causing overt activation or differences in B cell subset composition. We speculate that the impaired intestinal barrier function of NOD mice (49) could allow splenic B cells to be exposed to chronic, low-level stimulation by intestinal microbiota or their products or cytokines. Extensive further work will be required to test these possibilities.

In conclusion, these studies begin to define determinants of MHCII protein turnover in vivo, which include APC lineage, age, strain background, and environmental variables, but not, surprisingly, allelic polymorphism. Our findings overturn the long-standing, but controversial, hypothesis that autoimmunity in NOD mice arises from an inherent susceptibility of the disease-associated $A^{g7}$ allele to rapid turnover. Context, rather than structural MHCII polymorphism, determines the abnormal turnover of a proportion of $A^{g7}$ molecules in NOD mice. In B cells, which are essential for T1D (50) and harbor the great majority of splenic MHCII molecules, small differences in turnover among $A^d$, $A^{g7}$, and $E^d$ do not correlate with their effects on T1D risk. Accelerated $A^{g7}$ turnover in NOD splenic B cells declines with age before the onset of T1D in a low-incidence NOD colony and is not observed in a high-incidence NOD colony, indicating that fast $A^{g7}$ turnover is not required for T1D.

Our findings have broader implications. Any effects of genetic polymorphisms on protein turnover, as well as the role of protein turnover in genotype/phenotype relationships, are best evaluated in vivo, with due consideration of cellular and molecular heterogeneity. SINEW offers a widely applicable approach to this important problem.

## Acknowledgments

## Disclosures

## References

1. Makino, S., K. Kunimoto, Y. Muraoka, Y. Mizushima, K. Katagiri, and Y. Tochino. 1980. Breeding of a non-obese, diabetic strain of mice. *Jikken Dobutsu* 29: 1–13.
2. Hattori, M., J. B. Buse, R. A. Jackson, L. Glimcher, M. E. Dorf, M. Minami, S. Makino, K. Moriwaki, H. Kuzuya, H. Imura, et al. 1986. The NOD mouse: recessive diabetogenic gene in the major histocompatibility complex. *Science* 231: 733–735.
3. Lund, T., L. O'Reilly, P. Hutchings, O. Kanagawa, E. Simpson, R. Gravely, P. Chandler, J. Dyson, J. K. Picard, A. Edwards, et al. 1990. Prevention of insulin-dependent diabetes mellitus in non-obese diabetic mice by transgenes encoding modified I-A β-chain or normal I-E α-chain. *Nature* 345: 727–729.
4. Acha-Orbea, H., and H. O. McDevitt. 1987. The first external domain of the nonobese diabetic mouse class II I-A β chain is unique. *Proc. Natl. Acad. Sci. USA* 84: 2435–2439.
5. Busch, R., A. De Riva, A. V. Hadjinicolaou, W. Jiang, T. Hou, and E. D. Mellins. 2012. On the perils of poor editing: regulation of peptide loading by HLA-DQ and H2-A molecules associated with celiac disease and type 1 diabetes. *Expert Rev. Mol. Med.* 14: e15.
6. Todd, J. A., J. I. Bell, and H. O. McDevitt. 1988. HLA antigens and insulin-dependent diabetes. *Nature* 333: 710.
7. Cucca, F., R. Lampis, M. Congia, E. Angius, S. Nutland, S. C. Bain, A. H. Barnett, and J. A. Todd. 2001. A correlation between the relative predisposition of MHC class II alleles to type 1 diabetes and the structure of their proteins. *Hum. Mol. Genet.* 10: 2025–2037.
8. Suri, A., J. J. Walters, M. L. Gross, and E. R. Unanue. 2005. Natural peptides selected by diabetogenic DQ8 and murine I-A($^{g7}$) molecules show common sequence specificity. *J. Clin. Invest.* 115: 2268–2276.
9. Ridgway, W. M., H. Ito, M. Fassò, C. Yu, and C. G. Fathman. 1998. Analysis of the role of variation of major histocompatibility complex class II expression on nonobese diabetic (NOD) peripheral T cell response. *J. Exp. Med.* 188: 2267–2275.
10. Kanagawa, O., S. M. Martin, B. A. Vaupel, E. Carrasco-Marin, and E. R. Unanue. 1998. Autoreactivity of T cells from nonobese diabetic mice: an I-A$^{g7}$-dependent reaction. *Proc. Natl. Acad. Sci. USA* 95: 1721–1724.
11. Kouskoff, V., A. S. Korganow, V. Duchatelle, C. Degott, C. Benoist, and D. Mathis. 1996. Organ-specific disease provoked by systemic autoimmunity. *Cell* 87: 811–822.
12. Matsumoto, I., A. Staub, C. Benoist, and D. Mathis. 1999. Arthritis provoked by linked T and B cell recognition of a glycolytic enzyme. *Science* 286: 1732–1735.
13. Carrasco-Marin, E., J. Shimizu, O. Kanagawa, and E. R. Unanue. 1996. The class II MHC I-A$^{g7}$ molecules from non-obese diabetic mice are poor peptide binders. *J. Immunol.* 156: 450–458.
14. Ettinger, R. A., A. W. Liu, G. T. Nepom, and W. W. Kwok. 1998. Exceptional stability of the HLA-DQA1*0102/DQB1*0602 alpha beta protein dimer, the class II MHC molecule associated with protection from insulin-dependent diabetes mellitus. *J. Immunol.* 161: 6439–6445.
15. Reizis, B., M. Eisenstein, J. Bocková, S. Könen-Waisman, F. Mor, D. Elias, and I. R. Cohen. 1997. Molecular characterization of the diabetes-associated mouse MHC class II protein, I-A$^{g7}$. *Int. Immunol.* 9: 43–51.
16. Stratmann, T., V. Apostolopoulos, V. Mallet-Designe, A. L. Corper, C. A. Scott, I. A. Wilson, A. S. Kang, and L. Teyton. 2000. The I-A$^{g7}$ MHC class II molecule linked to murine diabetes is a promiscuous peptide binder. *J. Immunol.* 165: 3214–3225.
17. Ma, J. K., M. Y. Platt, J. Eastham-Anderson, J. S. Shin, and I. Mellman. 2012. MHC class II distribution in dendritic cells and B cells is determined by ubiquitin chain length. *Proc. Natl. Acad. Sci. USA* 109: 8820–8825.
18. Shin, J. S., M. Ebersold, M. Pypaert, L. Delamarre, A. Hartley, and I. Mellman. 2006. Surface expression of MHC class II in dendritic cells is controlled by regulated ubiquitination. *Nature* 444: 115–118.
19. Cella, M., A. Engering, V. Pinet, J. Pieters, and A. Lanzavecchia. 1997. Inflammatory stimuli induce accumulation of MHC class II complexes on dendritic cells. *Nature* 388: 782–787.
20. Rinderknecht, C. H., N. Lu, O. Crespo, P. Truong, T. Hou, N. Wang, N. Rajasekaran, and E. D. Mellins. 2010. I-A$^{g7}$ is subject to post-translational chaperoning by CLIP. *Int. Immunol.* 22: 705–716.
21. Rinderknecht, C. H., S. Roh, A. Pashine, M. P. Belmares, N. S. Patil, N. Lu, P. Truong, T. Hou, C. Macaubas, T. Yoon, et al. 2010. DM influences the abundance of major histocompatibility complex class II alleles with low affinity for class II-associated invariant chain peptides via multiple mechanisms. *Immunology* 131: 18–32.
22. Pashine, A., R. Busch, M. P. Belmares, J. N. Munning, R. C. Doebele, M. Buckingham, G. P. Nolan, and E. D. Mellins. 2003. Interaction of HLA-DR with an acidic face of HLA-DM disrupts sequence-dependent interactions with peptides. *Immunity* 19: 183–192.
23. Glazier, K. S., S. B. Hake, H. M. Tobin, A. Chadburn, E. J. Schattner, and L. K. Denzin. 2002. Germinal center B cells regulate their capability to present antigen by modulation of HLA-DO. *J. Exp. Med.* 195: 1063–1069.

24. Hornell, T. M., T. Burster, F. L. Jahnsen, A. Pashine, M. T. Ochoa, J. J. Harding, C. Macaubas, A. W. Lee, R. L. Modlin, and E. D. Mellins. 2006. Human dendritic cell expression of HLA-DO is subset specific and regulated by maturation. *J. Immunol.* 176: 3536–3547.

25. Chen, X., O. Laur, T. Kambayashi, S. Li, R. A. Bray, D. A. Weber, L. Karlsson, and P. E. Jensen. 2002. Regulated expression of human histocompatibility leukocyte antigen (HLA)-DO during antigen-dependent and antigen-independent phases of B cell development. *J. Exp. Med.* 195: 1053–1062.

26. Pozzilli, P., A. Signore, A. J. Williams, and P. E. Beales. 1993. NOD mouse colonies around the world—recent facts and figures. *Immunol. Today* 14: 193–196.

27. Lehuen, A., J. Diana, P. Zaccone, and A. Cooke. 2010. Immune cell crosstalk in type 1 diabetes. *Nat. Rev. Immunol.* 10: 501–513.

28. Markle, J. G., D. N. Frank, S. Mortin-Toth, C. E. Robertson, L. M. Feazel, U. Rolle-Kampczyk, M. von Bergen, K. D. McCoy, A. J. Macpherson, and J. S. Danska. 2013. Sex differences in the gut microbiome drive hormone-dependent regulation of autoimmunity. *Science* 339: 1084–1088.

29. Hou, T., C. H. Rinderknecht, A. V. Hadjinicolaou, R. Busch, and E. Mellins. 2013. Pulse-chase analysis for studies of MHC class II biosynthesis, maturation, and peptide loading. *Methods Mol. Biol.* 960: 411–432.

30. Krüger, M., M. Moser, S. Ussar, I. Thievessen, C. A. Luber, F. Forner, S. Schmidt, S. Zanivan, R. Fässler, and M. Mann. 2008. SILAC mouse for quantitative proteomics uncovers kindlin-3 as an essential factor for red blood cell function. *Cell* 134: 353–364.

31. De Riva, A., M. J. Deery, S. McDonald, T. Lund, and R. Busch. 2010. Measurement of protein synthesis using heavy water labeling and peptide mass spectrometry: Discrimination between major histocompatibility complex allotypes. *Anal. Biochem.* 403: 1–12.

32. Busch, R., Y. K. Kim, R. A. Neese, V. Schade-Serin, M. Collins, M. Awada, J. L. Gardner, C. Beysen, M. E. Marino, L. M. Misell, and M. K. Hellerstein. 2006. Measurement of protein turnover rates by heavy water labeling of nonessential amino acids. *Biochim. Biophys. Acta* 1760: 730–744.

33. Price, J. C., W. E. Holmes, K. W. Li, N. A. Floreani, R. A. Neese, S. M. Turner, and M. K. Hellerstein. 2012. Measurement of human plasma proteome dynamics with $^2H_2O$ and liquid chromatography tandem mass spectrometry. *Anal. Biochem.* 420: 73–83.

34. Rachdaoui, N., L. Austin, E. Kramer, M. J. Previs, V. E. Anderson, T. Kasumov, and S. F. Previs. 2009. Measuring proteome dynamics in vivo: as easy as adding water? *Mol. Cell. Proteomics* 8: 2653–2663.

35. Busch, R., R. A. Neese, M. Awada, G. M. Hayes, and M. K. Hellerstein. 2007. Measurement of cell proliferation by heavy water labeling. *Nat. Protoc.* 2: 3045–3057.

36. Herath, K., G. Bhat, P. L. Miller, S. P. Wang, A. Kulick, G. Andrews-Kelly, C. Johnson, R. J. Rohm, M. E. Lassman, S. F. Previs, et al. 2011. Equilibration of $^2H$ labeling between body water and free amino acids: enabling studies of proteome synthesis. *Anal. Biochem.* 415: 197–199.

37. Watts, T. H., A. A. Brian, J. W. Kappler, P. Marrack, and H. M. McConnell. 1984. Antigen presentation by supported planar membranes containing affinity-purified I-A$^d$. *Proc. Natl. Acad. Sci. USA* 81: 7564–7568.

38. Ozato, K., and D. H. Sachs. 1982. Detection of at least two distinct mouse I-E antigen molecules by the use of a monoclonal antibody. *J. Immunol.* 128: 807–810.

39. Ellis, S. A., C. Taylor, and A. McMichael. 1982. Recognition of HLA-B27 and related antigen by a monoclonal antibody. *Hum. Immunol.* 5: 49–59.

40. Barnstable, C. J., W. F. Bodmer, G. Brown, G. Galfre, C. Milstein, A. F. Williams, and A. Ziegler. 1978. Production of monoclonal antibodies to group A erythrocytes, HLA and other human cell surface antigens-new tools for genetic analysis. *Cell* 14: 9–20.

41. Erve, J. C., M. Gu, Y. Wang, W. DeMaio, and R. E. Talaat. 2009. Spectral accuracy of molecular ions in an LTQ/Orbitrap mass spectrometer and implications for elemental composition determination. *J. Am. Soc. Mass Spectrom.* 20: 2058–2069.

42. Xu, Y., J. F. Heilier, G. Madalinski, E. Genin, E. Ezan, J. C. Tabet, and C. Junot. 2010. Evaluation of accurate mass and relative isotopic abundance measurements in the LTQ-orbitrap mass spectrometer for further metabolomics database building. *Anal. Chem.* 82: 5490–5501.

43. Hellerstein, M. K., and R. A. Neese. 1999. Mass isotopomer distribution analysis at eight years: theoretical, analytic, and experimental considerations. *Am. J. Physiol.* 276: E1146–E1170.

44. Bluck, L. J. C., and W. A. Coward. 1997. Peak measurement in gas chromatographic/mass spectrometric isotope studies. *J. Mass Spectrom.* 32: 1212–1218.

45. King, C., A. Ilic, K. Koelsch, and N. Sarvetnick. 2004. Homeostatic expansion of T cells during immune insufficiency generates autoimmunity. *Cell* 117: 265–277.

46. Mariño, E., M. Batten, J. Groom, S. Walters, D. Liuwantara, F. Mackay, and S. T. Grey. 2008. Marginal-zone B-cells of nonobese diabetic mice expand with diabetes onset, invade the pancreatic lymph nodes, and present autoantigen to diabetogenic T-cells. *Diabetes* 57: 395–404.

47. Galbas, T., V. Steimle, R. Lapointe, S. Ishido, and J. Thibodeau. 2012. MARCH1 down-regulation in IL-10-activated B cells increases MHC class II expression. *Cytokine* 59: 27–30.

48. Mingueneau, M., W. Jiang, M. Feuerer, D. Mathis, and C. Benoist. 2012. Thymic negative selection is functional in NOD mice. *J. Exp. Med.* 209: 623–637.

49. Lee, A. S., D. L. Gibson, Y. Zhang, H. P. Sham, B. A. Vallance, and J. P. Dutz. 2010. Gut barrier disruption by an enteric bacterial pathogen accelerates insulitis in NOD mice. *Diabetologia* 53: 741–748.

50. Serreze, D. V., H. D. Chapman, D. S. Varnum, M. S. Hanson, P. C. Reifsnyder, S. D. Richard, S. A. Fleming, E. H. Leiter, and L. D. Shultz. 1996. B lymphocytes are essential for the initiation of T cell-mediated autoimmune diabetes: analysis of a new "speed congenic" stock of NOD.Ig mu null mice. *J. Exp. Med.* 184: 2049–2053.